Journal of Computational Physics 356 (2018) 448–457

Contents lists available at ScienceDirect

Journal of Computational Physics

www.elsevier.com/locate/jcp

Spectral treatment of gyrokinetic shear flow

J. Candy *, E.A. Belli

General Atomics, P.O. Box 85608, San Diego, CA 92186-5608, USA

ARTICLE INFO

Article history:
Received 15 August 2017
Received in revised form 9 December 2017
Accepted 14 December 2017
Available online 18 December 2017

Keywords:
Gyrokinetic
Shear
Flow

ABSTRACT

Sheared $\mathbf{E} \times \mathbf{B}$ flow in a tokamak, driven by external torque from neutral beam injection, is known to have an important stabilizing effect on drift-wave turbulence. In gyrokinetic codes, flow shear can be implemented directly on a radial mesh with nonperiodic boundary conditions. The mesh-based implementation is straightforward, but carries the possibility of spurious effects related to simulation boundaries. Alternatively, flow shear has been implemented in spectral solvers using a wavenumber shift method. Although the spectral representation has numerous computational benefits, the wavenumber shift method for treating flow shear is of questionable accuracy. Efforts to compare mesh-based solutions with spectral ones have met with limited success. In particular, significant differences in the critical shear required to stabilize turbulence are sometimes observed. We outline a new approach to treat flow shear spectrally. The method is simple to implement, matches the nonperiodic results more closely, and predicts a critical shear that is less sensitive to radial wavenumber resolution.

1. Introduction and background

1.1. History

External torque from neutral beam injection in tokamak plasmas can produce toroidal rotation velocities comparable to the ion sound speed. The radial variation (shear) in the corresponding $\mathbf{E} \times \mathbf{B}$ velocity is known to have an important stabilizing effect on drift-wave turbulence, thereby improving tokamak confinement. The importance of including this effect in nonlinear simulations of tokamak turbulence has long been known [1–5]. However, the way the effect is implemented depends on the simulation type; this can be either a radially-nonperiodic annulus [6], or a radially-periodic flux-tube [7]. In the former case, the shearing can be calculated simply and directly on a radial mesh with nonperiodic boundary conditions, such that calculated fluxes converge as the mesh is refined. In the latter case, however, the situation is more complicated. To understand the nature of this complication, note first that spectral flux-tube gyrokinetic solvers are computationally very efficient for certain problems since they work directly in wavenumber space and employ periodic radial and toroidal boundary conditions. In particular, simulations that require simultaneous resolution of electron-scale and ion-scale turbulence [8,9] benefit greatly from spectral algorithms. Unfortunately, periodic radial boundary conditions are fundamentally incompatible with flow shear. The standard method (herein called the *wavenumber-shift* method, and elsewhere called the *wavenumber-remapping* method [10]) gets around this problem by making use of the fact that toroidal harmonics return to radial periodicity at integer multiples of a critical time [11,12]. For a fixed radial domain size, however, the discretization

* Corresponding author.
E-mail address: candy@fusion.gat.com (J. Candy).

https://doi.org/10.1016/j.jcp.2017.12.020
0021-9991/

error is fixed and cannot be reduced by resolving higher wavenumbers. Thus, proving convergence via mesh refinement is not possible. Efforts to compare results from real-space and spectral implementations have been minimal, and in some cases significant differences in predictions of the critical shearing rate to stabilize turbulence have been observed [10,13]. In this work, we outline a new approach to the spectral shearing method that is very simple to implement, matches the global method more closely for a standard nonlinear test case, and predicts a critical shear that is relatively insensitive to wavenumber resolution.

1.2. Theoretical considerations

In the recursive formulation of nonlinear electromagnetic gyrokinetic theory [14,15], fluctuations are represented in eikonal (ballooning) form as

$$h_a(\mathbf{R}) = \sum_{\mathbf{k}_\perp} e^{iS_{\mathbf{k}}(\mathbf{R},t)} h_{a,\mathbf{k}_\perp} \,, \tag{1}$$

where $\mathbf{k}_\perp \doteq \nabla_\perp S_{\mathbf{k}}$ is the perpendicular wavenumber, $\mathbf{R}$ is the location of a gyrocenter, and a is the species index. When the plasma has a flow velocity $\mathbf{V}_0$, the eikonal becomes time dependent [16,2,14,15], such that

$$\frac{\partial S_{\mathbf{k}}}{\partial t} = -\mathbf{k}_\perp \cdot \mathbf{V}_0 \,. \tag{2}$$

In a tokamak, any mean flow on the order of a thermal ion velocity must be purely toroidal and of the form $\mathbf{V}_0 = R^2\omega_0(\psi)\nabla\varphi$ [17]. In terms of the nonrotating part of the eikonal, $S_{\mathbf{k}}(0)$, we have

$$S_{\mathbf{k}}(t) = S_{\mathbf{k}}(0) + n\omega_0 t \,, \tag{3}$$

$$\mathbf{k}_\perp(t) = \mathbf{k}_\perp(0) + n\nabla r \frac{\partial \omega_0}{\partial r} t \,, \tag{4}$$

where $n \doteq -R^2\mathbf{k}_\perp \cdot \nabla\varphi$, and r is the *midplane minor radius* (the half-width of the flux surface at the elevation of the centroid [18]). In this paper, we use the non-orthogonal field-aligned coordinate system (ψ, θ, α) together with the Clebsch representation for the magnetic field [19], $\mathbf{B} = \nabla\alpha \times \nabla\psi$. Here, $\alpha \doteq \varphi + \nu(\psi,\theta)$, where φ is the toroidal angle, ψ is the poloidal flux divided by 2π, and θ is the poloidal angle. The safety factor, q, is defined as

$$q(\psi) \doteq \frac{1}{2\pi}\int_0^{2\pi} \frac{\mathbf{B}\cdot\nabla\varphi}{\mathbf{B}\cdot\nabla\theta}\, d\theta = \frac{1}{2\pi}\int_0^{2\pi}\left(-\frac{\partial\nu}{\partial\theta}\right) d\theta = \frac{\nu(\psi,0)-\nu(\psi,2\pi)}{2\pi} \,. \tag{5}$$

With these results, the eikonal can be put into a more useful and intuitive form by introducing the *poloidal wavenumber* $k_\theta = nq/r$ and the *Waltz shearing rate* [1],

$$\gamma_E \doteq -\frac{r}{q}\frac{d\omega_0}{dr} \,, \tag{6}$$

to yield

$$S_{\mathbf{k}}(t) = S_{\mathbf{k}}(0) + n\omega_0(r_0)t - (r-r_0)k_\theta\gamma_E t \,, \tag{7}$$

$$\mathbf{k}_\perp(t) = \mathbf{k}_\perp(0) - \nabla r k_\theta \gamma_E t \,. \tag{8}$$

To arrive at this result, we have expanded the rotation frequency ω_0 about the center of the simulation domain $r = r_0$:

$$\omega_0 \sim \omega_0(r_0) + \left[\frac{d\omega_0}{dr}\right]_{r=r_0} (r-r_0) \,. \tag{9}$$

In what follows we will neglect the $\omega_0(r_0)$ term in Eq. (7) since it represents a simple Doppler shift in the frequency.

2. Periodic and nonperiodic series

For numerical simulation, fluctuations for plasma species a can in principle be decomposed using an explicit double Fourier series with *time-dependent* eikonal

$$h_a(x,\alpha,t) = f_{0a}\sum_{n=-N}^{N}\sum_{p=-M}^{M} e^{ipx}e^{-ix\gamma_s t}e^{-in\alpha}\,\widehat{h}_a(n,p,t) \,. \tag{10}$$

This representation implies $\mathrm{S}_{\mathbf{k}}(t) = (p - \gamma_s t)x - n\alpha$. However, in practice this decomposition is not used; rather, an expansion in terms of a *time-independent* eikonal is preferred

$$h_a(x, \alpha, t) = f_{0a} \sum_{n=-N}^{N} \sum_{p=-M}^{M} e^{ipx} e^{-in\alpha} \widetilde{h}_a(n, p, t) \,, \tag{11}$$

where $\mathrm{S}_{\mathbf{k}}(0) = px - n\alpha$. In these expressions, f_{0a} is the zeroth-order equilibrium Maxwellian distribution for species a. The time-independent representation in Eq. (11) is clarified further in Section 3 of Ref. [20]. In both Eqs. (10) and (11), we have defined an angular radial variable $x = 2\pi(r - r_0)/L \in [0, 2\pi)$, where L is the radial width of the simulation domain. The *domain shearing rate*, defined as

$$\gamma_s \doteq \frac{k_\theta L}{2\pi} \gamma_E \,, \tag{12}$$

increases as L is increased at fixed shearing rate. Inspection of Eq. (10) indicates that the shear flow manifests itself as an apparent time-dependence of the radial wavenumber: $p - \gamma_s t$. The presence of shear flow makes $h_a(x, \alpha, t)$ nonperiodic in x and significantly complicates the approach to numerical simulation. Note however that if one transforms to a frame moving with the flow, $x' = x$, $\alpha' = \alpha + x(\gamma_s/n)t$, then Eq. (10) can be interpreted as a periodic representation in the moving coordinates. Working in this periodic, moving frame is the basis of the popular method, developed by Rogallo [21], for simulating homogeneous turbulent shear flow in fluids. In Rogallo's approach, the time-dependent wavenumber is retained in the fluid equations, and the system periodically *remeshed* in order to counteract the deformation of the moving frame with respect to the stationary frame. In Fourier space, the remeshing is equivalent to shifting wavenumbers [22]. We will describe this shifting approach in more detail below. Because the remeshing step can lead to a significant loss of turbulent kinetic energy in fluid simulations, sometimes the remeshing is avoided and the simulation carried out in the highly-deformed sheared coordinates.

Ultimately, Eqs. (10) and (11) represent two fundamentally different representations for the distribution; the former is nonperiodic in x, whereas the latter is periodic. To clarify the differences, we summarize the various representations of the nonlinear gyrokinetic equation. First, the real-space form is written symbolically as

$$\textbf{Real-space, nonperiodic with flow:} \qquad \frac{\partial h_a}{\partial t} = ix\gamma_s h_a + G \,, \tag{13}$$

where G represents the total righthand side of the nonlinear gyrokinetic equation. The effect of flow in this case is included explicitly as a nonperodic shearing term $ix\gamma_s h_a$, and the solution h_a is a nonperiodic function. When writing the equation in this form, the principle difficulty is related to development of efficient boundary conditions (see Chapter 7, Ref. [23]), whereas treatment of the shearing term itself is straightforward. The spectral gyrokinetic equation *with shear flow*, based on the expansion in Eq. (10), takes the symbolic form

$$\textbf{Spectral, nonperiodic with flow:} \qquad \frac{\partial \widehat{h}_a}{\partial t} = \mathcal{G}(n, p - \gamma_s t, \widehat{h}_a) \,. \tag{14}$$

To clarify the meaning of this equation, we emphasize that no explicit shearing term appears in $\mathcal{G}$; instead, the effect of flow shear is captured entirely by the time-dependent wavenumber. This representation has been used with success for the short-time simulation of ordinary fluids by Brucker [24], with negligible added cost required to implement a time-dependent wavenumber in the Navier–Stokes equations. Unfortunately, due to their complexity, existing flux-tube gyrokinetic solvers have only been formulated using some variation of the periodic, time-independent spectral representation, Eq. (11). Certainly, the case **without shear** can be treated this way by solving the equation

$$\textbf{Spectral, periodic without flow:} \qquad \frac{\partial \widetilde{h}_a}{\partial t} = \mathcal{G}(n, p, \widetilde{h}_a) \,. \tag{15}$$

The above form, Eq. (15), describes the way that CGYRO is formulated, as written in Eq. (57) of Ref. [20]. We can make contact with Ref. [20] by writing

$$\left(\frac{a}{c_s}\right) \mathcal{G}(n, p, \widetilde{h}_a) \doteq i\left(\Omega_\theta + \Omega_\xi + \Omega_{\mathrm{d}}\right) \widetilde{H}_a + i\Omega_* \widetilde{\Psi}_a - \frac{2\pi a}{L} \frac{q\rho_s}{r} \widetilde{h}_a * \widetilde{\Psi}_a + \frac{a}{c_s} \sum_b C_{ab}^L \left(\widetilde{H}_a, \widetilde{H}_b\right) \,, \tag{16}$$

where $c_s = \sqrt{T_e/m_{\mathrm{D}}}$ is the deuteron sound speed, T_e is the electron temperature, and m_{D} is the deuteron mass. Explicit forms for $\widetilde{H}_a$, Ω_θ, Ω_ξ, Ω_{d}, Ω_*, $\widetilde{\Psi}_a$, C_{ab}^L and $*$ (a generalized convolution) are given in Ref. [20].

So, the situation presents a conundrum: in the limit of no flow shear, numerical gyrokinetic solvers for the spectral equations are relatively simple, have low truncation error, and are free of complex, artificial radial boundary conditions. Conversely, flow shear can be represented spectrally in a conceptually simple way using the time-dependent wavenumber $p - \gamma_s t$, but a direct numerical implementation is judged to be computationally prohibitive. For example, many expensive

function evaluations which are normally precomputed would need to be recalculated every timestep. For this reason, no codes (to our knowledge) implement a time-dependent wavenumber in $\mathcal{G}$. Early particle-in-cell simulations by Dimits [3] employed sheared coordinates to treat equilibrium flow, but with a nonspectral representation in real space.

2.1. Existing global implementations on a radial mesh

As previously explained, if the equations are solved on a radial mesh using nonperiodic boundary conditions, it is straightforward to implement the shear explicitly as in Eq. (13). This is the numerical approach used in GYRO [6] and more recently in GKW [25]. A significant number of nonlinear simulations were carried out using the nonperiodic GYRO implementation by Kinsey [26,27] in order to inform the development of an $\mathbf{E}\times\mathbf{B}$ shear quench rule for the TGLF model [28].

2.2. Wavenumber shift method

As noted above, retaining the time-dependent wavenumber $p-\gamma_s t$ in $\mathcal{G}$ would in principle allow solution of the problem. Indeed, the time-dependent wavenumber approach has been used with success to treat homogeneous turbulent shear flow in ordinary fluids [24], but as we have noted, it would introduce a significant computational expense to existing flux-tube gyrokinetic codes. For example, all $\mathbf{k}_\perp$-dependent terms, particularly the Bessel functions associated with gyroaveraging, would need to be recomputed for every timestep. For this reason, the shearing is normally implemented using an approximate *wavenumber shift method* developed by Hammett and coworkers [11]. The shift method makes use of the observation that the system will return to periodicity after a time $\Delta t = 1/\gamma_s$. To implement this approach, we note at time $t=0$, the radial dependence for a single value of n is

$$\sum_p \widehat{h}(n,p,0)e^{ipx}\,. \tag{17}$$

After a time Δt, the system evolves to

$$\sum_p \widehat{h}(n,p,\Delta t)e^{ipx}e^{-ix\gamma_s\Delta t} = \sum_p \widehat{h}(n,p,\Delta t)e^{i(p-1)x} = \sum_p \widehat{h}(n,p+1,\Delta t)e^{ipx}. \tag{18}$$

Thus, after a time Δt, the $(p+1)$th amplitude has both evolved according to Eq. (14) and shifted into the position of the pth amplitude. The essence of the wavenumber shift method is to account for this shift, but to approximate $\mathcal{G}(n,p-\gamma_s t,\widehat{h})$ by $\mathcal{G}(n,p,\widehat{h})$ for $0\le t\le 1/\gamma_s$. In other words, the time-dependence of $\mathbf{k}_\perp$ in $\mathcal{G}$ is ignored, and wavenumbers are shifted after each Δt time interval (i.e., a Rogallo-type remesh but neglecting the time-dependent wavenumber in $\mathcal{G}$). The boundary conditions to be applied after each shift are $\widehat{h}(n,p,t)=0$ for $|p|>M$. This algorithm is simple to implement and imposes a negligible cost on the simulation. Unfortunately, it is not possible to demonstrate convergence of this algorithm using standard mesh-refinement techniques. One can approach the continuum limit only by taking $L\to\infty$, whereas at finite L there is a fixed, irreducible error. No rigorous error analysis has been attempted, thus the hope is that the dominant effect of shear is captured by the amplitude shift while neglect of the time-dependence of the wavenumber represents a relatively smaller error.

The wavenumber shift method has been previously implemented in numerous flux-tube codes including GKW [12], GS2 [29,30] and GENE [31], and subsequently employed for physics studies [32,10,33]. Although some work has been done to assess the accuracy of the method, no definitive analysis of the properties of the algorithm has been published. The most detailed numerical studies have been carried out by Casson [10] who presents numerous radial and binormal resolution scans. The key findings are: (a) the critical shear at which turbulence is quenched varies significantly as binormal resolution is changed, (b) the agreement between global GYRO and flux-tube GKW results is marginal.

We remark that the shift method has an additional negative aspect; namely, that the time-history of simulations is discontinuous due to the discrete nature of the shift algorithm. This means that time-dependent curves of fluctuations, transport coefficients, simulation error, etc, will show small discontinuities at times where the shifts are implemented. Nevertheless, Fig. 1 indicates that the method is in reasonably good agreement with GYRO. Specifically, plots of the ion energy flux, Q_i, and ion momentum flux, Π_i, versus shearing rate γ_E are shown, comparing global GYRO simulations (with nonperiodic boundary conditions) with flux-tube CGYRO simulations (with the wavenumber shift method). We give the general definitions of the various fluxes in Appendix A, and summarize the nonlinear simulation parameters in Appendix B. The shift method is shown to perform well for intermediate shearing rates, but exhibits a spurious increase in Q_i at low shearing rate and overestimates the turbulence quench point at high shearing rate. The overestimate of the location of the quench point has previously been observed by Casson (see Fig. 4 of Ref. [10]). As Casson has also shown, and we have verified, the flux will eventually collapse. However, the critical shear for this collapse is highly dependent on resolution and for this reason we do not extend the plot out to the quench point. Hammett [11] asserts that the method should be well-converged if $\gamma_E \gg \gamma_L$, where γ_L is a measure of the linear growth rate. This estimate is consistent with the increasing discrepancy in Q_i (see Fig. 1) as $\gamma_E\to 0$. The momentum flux trend is well-reproduced by the wavenumber-shift method, but the magnitude is about 20% higher than the GYRO prediction. We believe it is more likely that these differences are due

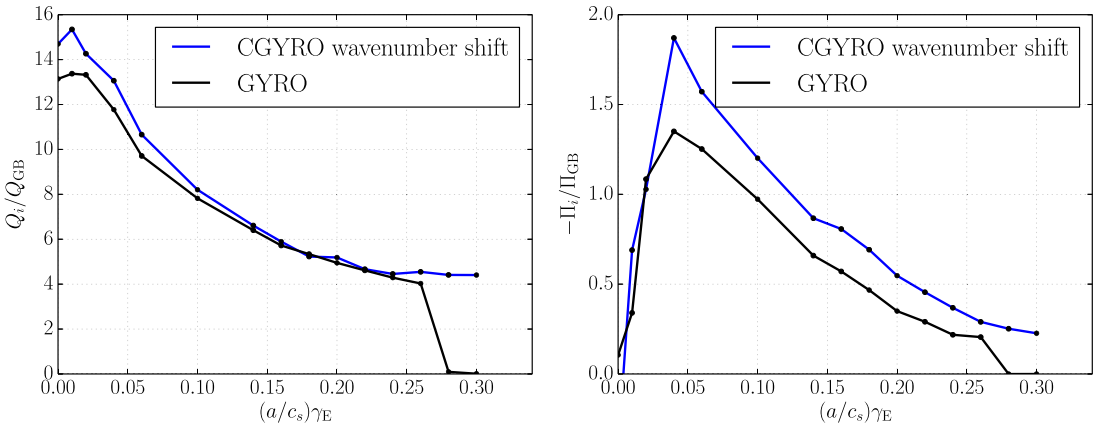

Fig. 1. Ion energy flux, Q_i, and ion momentum flux, Π_i, versus shearing rate γ_E for the GA standard case parameters [1] (see Appendix B). Reference global GYRO simulations with nonperiodic boundary conditions are shown in black. Flux-tube CGYRO simulations with the wavenumber shift (Hammett) method are shown in blue. The latter agree very well with GYRO for intermediate shearing rates, but exhibit a spurious increase in Q_i at low shearing rate, and over-estimate the quench point at high shearing rate. The momentum flux trend is well-reproduced by the wavenumber-shift method, but the magnitude is about 20% higher than the GYRO prediction. (For interpretation of the references to color in this figure legend, the reader is referred to the web version of this article.)

to inaccuracies of the shift method rather than inaccuracies in the GYRO solution. This is a speculation that we will attempt to further justify.

3. A new wavenumber advection method

As an alternative to the wavenumber shift method, we wish to treat the shearing term explicitly, in the spirit of the nonperiodic real-space formulation of Eq. (13), but using the spectral, time-independent representation of fluctuations defined in Eq. (11). We do this by employing a *periodization* of the nonperiodic function x. Then we can write a periodic spectral GK equation with flow shear as

$$\textbf{Spectral, periodic with flow:} \qquad \frac{\partial \widetilde{h}_a}{\partial t} = i\gamma_s X \widetilde{h}_a + \mathcal{G}(n, p, \widetilde{h}_a)\,. \tag{19}$$

The operator X is defined in accordance with a real-space sine series

$$x \sim x_{\rm P}(x) \doteq 2\sum_k a_k \sin(kx)\,, \tag{20}$$

where $x_{\rm P}(x)$ is the *periodized shearing profile*. According to this periodization, the spectral shearing operator is

$$iX\widetilde{h}(p) \doteq \sum_k a_k \left[\widetilde{h}(p-k) - \widetilde{h}(p+k)\right]\,, \tag{21}$$

where above, and hereafter, we suppress dependence on the species and toroidal wavenumber. Symbolically, X is represented as an antisymmetric matrix, whereas in a numerical simulation it is implemented in the same way as a finite-difference stencil.

3.1. Taylor methods

It now remains to determine the optimal choice for the coefficients a_k. The simplest approach is to choose the a_k so that the Taylor expansion of

$$x - 2a_1\sin(x) + 2a_2\sin(2x) + 2a_3\sin(3x) + \cdots \tag{22}$$

about $x = 0$ vanishes to a given order. Choosing $a_1 = 1/2$ and $a_k = 0$ for $k > 1$ generates the *2nd-order Taylor method*,

$$\frac{\partial \widetilde{h}(p)}{\partial t} + \frac{\gamma_s}{2}\left[\widetilde{h}(p+1) - \widetilde{h}(p-1)\right] = \mathcal{G}(p)\,. \tag{23}$$

It is interesting to note that this is equivalent to the 2nd-order centered difference approximation to the continuous one-way wave equation

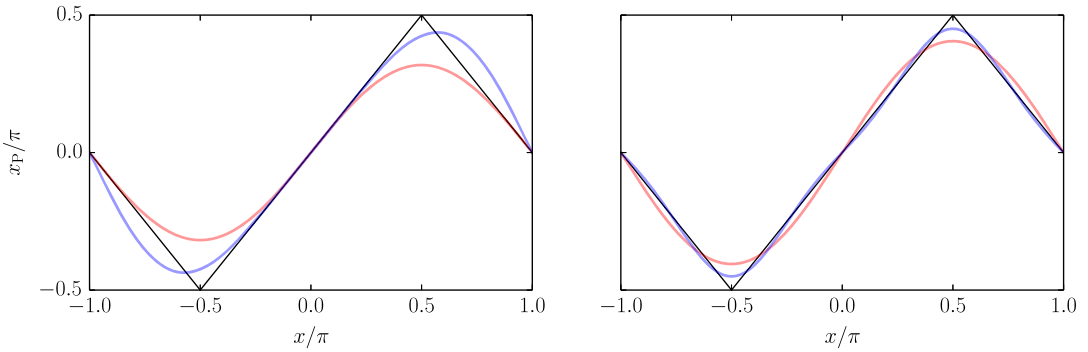

Fig. 2. Periodized shearing functions, x_P, as defined in Eq. (20). Plot (a) shows the 2nd (red) and 4th (blue) order Taylor approximations, and plot (b) shows the 1-term (red) and 2-term (blue) Fourier triangle approximation. (For interpretation of the references to color in this figure legend, the reader is referred to the web version of this article.)

$$\frac{\partial \widetilde{h}}{\partial t} + \gamma_s \frac{\partial \widetilde{h}}{\partial p} = \mathcal{G}(p) \,. \tag{24}$$

More generally, matching the Taylor polynomials to successively higher order gives difference equations which are the exact analogs of higher-order finite-difference discretizations to the continuous one-way wave equation. For example, matching up to $\mathcal{O}(x^3)$ gives $a_1 = 2/3$ and $a_2 = -1/12$, which is the *4th-order Taylor method*, or equivalently the 4th-order centered difference approximation to the continuous wave equation. We plot the periodized functions $x_P(x)$ for the 2nd and 4th-order Taylor approximations in Fig. 2. Although the approach might appear promising, nonlinear simulations indicate that the Taylor methods, instead of converging with order, give progressively greater suppression of transport as the order is increased. The 6th and higher-order methods perform badly and thus Taylor methods are *not recommended*.

3.2. Triangle methods

As an alternative to the Taylor methods – and motivated by the known result that the stabilization of turbulence is insensitive to the sign of γ_s (when the linear spectrum is symmetric in p) [34] – we set x_P equal to the partial Fourier-series representation of a triangle wave, $T(x)$, where

$$T(x) = \sum_{k=1,3,5,\ldots} \frac{4}{\pi k^2} \sin(kx) \,. \tag{25}$$

The triangle wave has constant magnitude of the shearing rate, namely $|dT/dx| = 1$ (except at the corners) but is periodic and continuous. The series convergence is also rapid and, because the underlying function is continuous, there is no Gibbs phenomenon. Thus, in a qualitative sense, the triangle method represents two simulations: one with positive shear and one with negative shear. However, as we will discuss shortly, some long-range correlations are induced by zonal flows. Proceeding, we can numerically implement the *1-term triangle method* according to

$$\frac{\partial \widetilde{h}(p)}{\partial t} + \frac{2\gamma_s}{\pi} \left[\widetilde{h}(p+1) - \widetilde{h}(p-1)\right] = \mathcal{G}(p) \,. \tag{26}$$

Comparison with Eq. (23) shows that the 1-term triangle method is equivalent to the 2nd-order Taylor method, but with an effective shearing rate of $(4/\pi)\gamma_s \simeq 1.27\,\gamma_s$. The *2-term triangle method* takes the form

$$\frac{\partial \widetilde{h}(p)}{\partial t} + \frac{2\gamma_s}{\pi} \left[\widetilde{h}(p+1) - \widetilde{h}(p-1)\right] - \frac{2\gamma_s}{9\pi} \left[\widetilde{h}(p+3) - \widetilde{h}(p-3)\right] = \mathcal{G}(p) \,. \tag{27}$$

Because retaining only 2 terms in the Fourier series yields a very good global approximation to $T(x)$, as shown in Fig. 2, our expectation is that the 2-term triangle method will be sufficient for simulation purposes. This limitation serves to avoid excessively wide difference stencils, and also to ensure that the shearing is driven by only the two longest (equilibrium-scale) waves in the system. Nonlinear tests (not shown) yield very minor differences between 2 and 3-term results. However, before showing numerical results for the triangle method, further modifications are required. Implementation of the new advection term has roughly the same computational requirements as implementing the wavenumber-shift method. As long as wavenumbers are not distributed in memory (i.e., by MPI), the added computational cost is insignificant.

3.3. Momentum transport and zonal mode filtering

With a straightforward implementation of the triangle method, the calculation of energy flux is relatively accurate. This was an a priori expectation since, as discussed in the previous section, the energy flux is insensitive to the sign

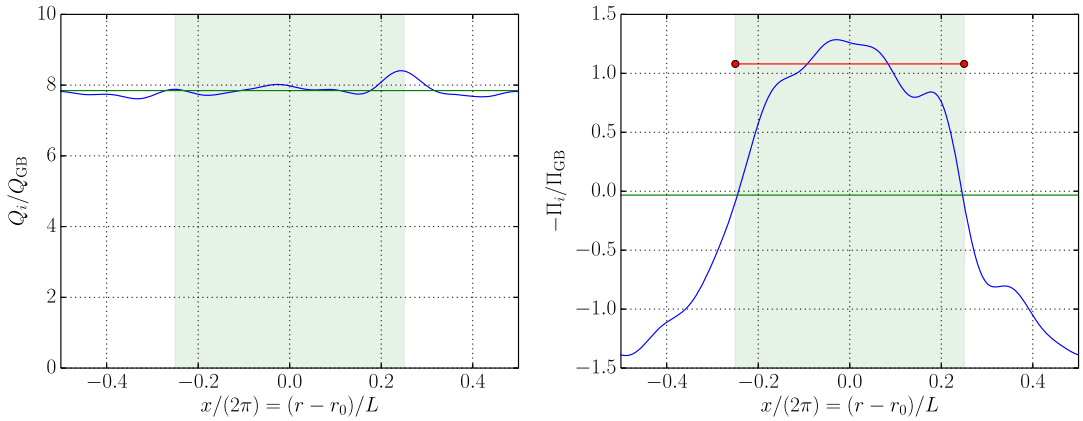

Fig. 3. Illustration of radial dependence of energy and momentum fluxes for shearing rate $\gamma_E = 0.1$. The green shaded zone shows the physical shearing region. Green horizontal lines show the full-domain averages. For the momentum flux, we estimate the value over physical region using the overshoot method; namely, the amplitude of the $\cos x$ component of the flux divided by $4/\pi$. This value is shown in red. (For interpretation of the references to color in this figure legend, the reader is referred to the web version of this article.)

of γ_E (it is exactly invariant for the simple up-down-symmetric flux-surface shape studied here). However, the sign of the $\mathbf{E}\times\mathbf{B}$-shear-generated momentum flux depends on the sign of γ_E [34,35], so simulations with the triangle method give rise to profiles of momentum flux with the correct sign over half of the simulation domain, and the opposite sign over the other half; that is, with an approximate $\cos x$ shape. While one could compute the momentum flux by a partial-domain average (for example, an average over the region $x \in [-0.2, 0.2]$), we can alternatively use an approximation based on the Fourier triangle expansion. Since the derivative of the triangle function is the step function, we expect that the $\cos x$ part of the flux will *overshoot* the total flux by the correction factor $4/\pi$ of Sec. 3.2. The average as determined by the overshoot estimate is illustrated in Fig. 3. We also computed the momentum flux by partial-domain average and the result is within 2% of the overshoot method. The formal approach used to compute radially-dependent fluxes is outlined in Appendix A.

Numerical simulations indicate that the partial domain average will yield the correct γ_E-driven momentum flux, but only in the limit of very large domain sizes L – much larger than that required to obtain a well-converged energy flux. The need for excessively large L is related to excitation of the two longest-wavelength zonal harmonics: $(n, p) = (0, \pm 1)$. In unsheared flux-tube simulations that are converged with respect to box size, these modes represent negligible long-scale correlations. Thus the filtering process prevents spurious generation of these modes. The filter we propose will typically give rise to only a small correction to the momentum flux. The method modifies the equations for $(n, p) = (0, 1)$ and $(0, -1)$ according to

$$\frac{\partial \widetilde{h}_a(0,1,t)}{\partial t} + \eta\,|\gamma_E|\left[\widetilde{h}_a(0,1,t) - \widetilde{h}_a(0,-1,t)\right] = \mathcal{G}(0,1,\widetilde{h}_a)\,, \tag{28}$$

$$\frac{\partial \widetilde{h}_a(0,-1,t)}{\partial t} + \eta\,|\gamma_E|\left[\widetilde{h}_a(0,-1,t) - \widetilde{h}_a(0,1,t)\right] = \mathcal{G}(0,-1,\widetilde{h}_a)\,, \tag{29}$$

where $\widetilde{h}_a = \widetilde{h}_a(n, p, t)$. The damping terms can be implemented straightforwardly using the same time integrator as for the unsheared part of the problem, with no need for operator splitting or other techniques. With this correction, one can follow the standard box-size convergence tests required by standard gyrokinetics. Note that the $\mathbf{E}\times\mathbf{B}$ shearing term does not appear in Eqs. (28) or (29) because $\gamma_s = 0$ for $n = 0$. Subtracting the two equations shows that only the longest-wavelength antisymmetric zonal mode is damped. We find that a scaling parameter $\eta = 0.2$ is adequate, and results essentially invariant for $\eta > 0.2$. With this zonal-damping correction implemented, the agreement between GYRO (global nonperiodic) and CGYRO (spectral periodic) – for both the energy and momentum fluxes – is excellent, as shown in Fig. 4. Note that for the chosen domain size, the periodic CGYRO simulations give a slightly larger flux than the nonperiodic GYRO simulations at $\gamma_E = 0$. The nominal interpretation is that there is a small amount of spurious shear in the GYRO simulations due to the nonperiodic boundary conditions. This effect is quickly washed away as γ_E increases.

For realistic tokamak parameters, the γ_E-driven momentum flux is significantly smaller than that driven by the parallel velocity shear, γ_p [34]. Moreover, the shear γ_p is easily implemented in a periodic flux-tube with usual methods. Similarly, momentum flux can also be driven by up-down asymmetric flux-surface geometry, as well as other rotation terms like the Coriolis drift and centrifugal force. Although these added terms will predominantly introduce a radially-constant offset to the momentum flux, there are subtle aspects to the dynamics that preclude use of the overshoot method. Thus the partial-domain average should be used in the general case for computing fluxes in all transport channels. Although we have verified the accurate performance of the present scheme for finite γ_p by comparison with GYRO, we defer presentation of the results to a subsequent publication.

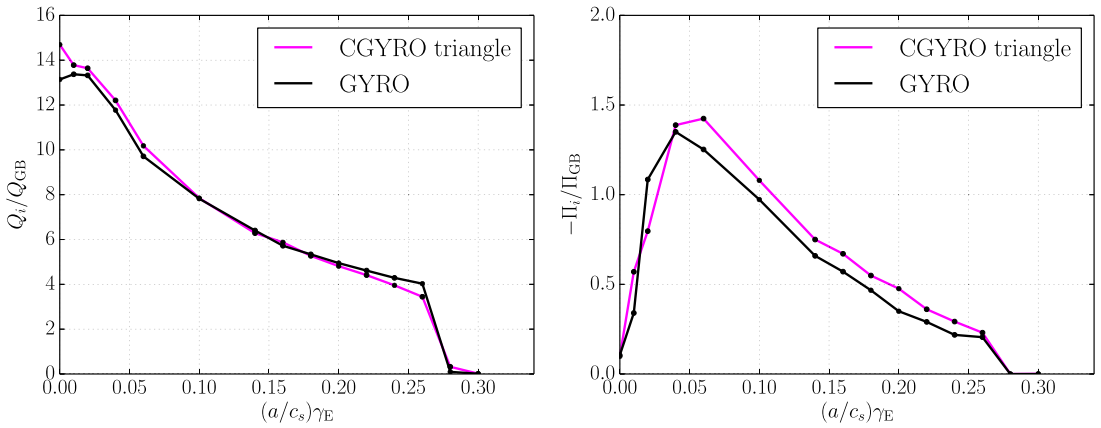

Fig. 4. Ion energy flux, Q_i, and ion momentum flux, Π_i, versus shearing rate γ_E for the GA standard case parameters. Reference global GYRO simulations with nonperiodic boundary conditions are shown in black. Flux-tube CGYRO simulations with the 2-term triangle method are shown in magenta. Both the momentum and energy fluxes are in good agreement despite the use of different codes and significantly different algorithms and boundary conditions. (For interpretation of the references to color in this figure legend, the reader is referred to the web version of this article.)

3.4. Sawtooth method

For completeness, we note that yet another – perhaps obvious – choice would be to replace x by its periodic extension; that is, to choose a sawtooth wave as the periodization $x_{\rm P}(x)$. In fact, the sawtooth representation is not new and has been considered in theoretical treatments of the shear stabilization problem [36] and also implemented in nonlinear gyrofluid simulations [1]. While the sawtooth wave has the virtue of maintaining a single sign of the shear over most of the domain, it introduces a region of very high shear at the point of discontinuity. Moreover, the Fourier series for a sawtooth wave converges slowly (the coefficients decay as $a_k \sim 1/k$ because of the discontinuity) and the waveform exhibits Gibbs phenomena there. When applied to the GA standard case, the sawtooth representation gives far too much turbulence stabilization. More specifically, for the nonlinear case of Fig. 1, the sawtooth method leads to complete stabilization by $\gamma_E = 0.1$. This is a significant error and indicates the sawtooth method should not be used.

4. Summary

The wavenumber advection method described in this work offers a new approach for the inclusion of $\mathbf{E} \times \mathbf{B}$ shear in flux-tube simulation of tokamak plasmas. By treating the shear explicitly as a difference operator on the discrete wavenumber grid, the effect of shear can be included simply and accurately. The method overcomes three principal disadvantages of the existing wavenumber shift method. First, a spurious increase in flux at low $\mathbf{E} \times \mathbf{B}$ shear seems to be eliminated; second, the value of γ_E at which turbulence is fully quenched is in better agreement with nonperiodic simulations; and third, discontinuities in the time-history of the simulation are eliminated. The last result is critical if one wishes to integrate the gyrokinetic equations with a linear multi-step time integrator. We recommend the 2-term triangle method, Eq. (27), because it strikes a good balance between accuracy and a compact stencil width.

Not only is the method suitable for the simulation of electric field shear, but the method can, in principle, be directly adapted to the simulation of shear in the temperature and density profiles [35] – stabilizing mechanisms which may be important for pedestal gyrokinetic simulations. At the same time, because the approach is spectral, the use of *ad hoc* radial boundary conditions are avoided and the entire domain is treated with spectral accuracy. This too makes the present approach suitable for pedestal multiscale simulations that treat ion-scale and electron-scale turbulence simultaneously.

Acknowledgements

The authors would like to thank R. Waltz and G. Staebler for helpful comments and suggestions. This material is based upon work supported by the U.S. Department of Energy, Office of Science, Office of Fusion Energy Sciences, Theory program under award DE-FG02-95ER54309, by the Center for the Study of Plasma Microturbulence under Award DE-FC02-08ER54963, and by the Edge Simulation Laboratory project under Grant DE-FC02-06ER54873. An award of computer time was provided by the Innovative and Novel Computational Impact on Theory and Experiment (INCITE) program. This research used resources of the Oak Ridge Leadership Computing Facility located in the Oak Ridge National Laboratory, which is supported by the Office of Science of the Department of Energy under Contract DE-AC05-00OR22725.

Appendix A. Global flux profile

The fluxes of particles (Γ_a), momentum (Π_a) and energy (Q_a) have the universal structure

$$F(x,\alpha) = \left\langle \int d^3v\; w_a(\mathbf{R}) H_a(\mathbf{R})^* \right\rangle \tag{30}$$

where the angle brackets denote a flux-surface average, defined as

$$\langle\cdots\rangle \doteq \frac{\oint d\theta\, d\varphi\, \mathcal{J}_\psi \cdots}{\oint d\theta\, d\varphi\, \mathcal{J}_\psi} . \tag{31}$$

In these coordinates, the Jacobian determinant is $\mathcal{J}_\psi \doteq (\nabla\psi \times \nabla\theta \cdot \nabla\alpha)^{-1}$. Explicit expressions for w_a are given in Eq. (49) of Ref. [15]. More specifically, in the latter reference, $\hat{w}_{a1}$ gives the particle flux, $\hat{w}_{a2}$ the heat flux, $\hat{w}_{a3}$ the momentum flux, and $\hat{w}_{a4}$ the anomalous exchange. By averaging over the binormal direction we obtain the radial flux profile

$$F(x) = \int \frac{d\alpha}{2\pi} F(x,\alpha) = \sum_\ell e^{i\ell x} F_\ell \tag{32}$$

where reality requires $F_\ell = F^*_{-\ell}$. Some algebra shows

$$F_\ell = \sum_{n,p} \left\langle \int d^3v\; f_{0a} \widetilde{H}^*_a(n,p) \widetilde{w}_a(n,p+l) \right\rangle , \tag{33}$$

where

$$w_a(\mathbf{R}) = \sum_{n,p} e^{ipx} e^{-in\alpha}\, \widetilde{w}_a(n,p) . \tag{34}$$

These Fourier coefficients can be used to reconstruct the radial flux profile $F(x)$. Normally, in a flux-tube simulation, only the mean flux is reported; this is

$$F_0 = \sum_{n,p} \left\langle \int d^3v\; f_{0a}\, \widetilde{H}^*_a(n,p) \widetilde{w}_a(n,p) \right\rangle . \tag{35}$$

The total ensemble-averaged flux [37] can then be obtained by computing a time-average of F_0.

Appendix B. Nonlinear simulation parameters and resolution

The physical case simulated with both GYRO and CGYRO is the General Atomics (GA) standard case [4] with adiabatic electrons: $R_0/a = 3$, $r/a = 0.5$, $q = 2$, $T_i = T_e$, $a/L_{ni} = 1$, $a/L_{Ti} = 3$. Here, the temperature and density gradient inverse scale lengths are defined as

$$\frac{1}{L_{Ta}} = -\frac{d\ln T_a}{dr} \quad \text{and} \quad \frac{1}{L_{na}} = -\frac{d\ln n_a}{dr} . \tag{36}$$

The gradients in the toroidal velocity are taken to be zero (i.e., $\gamma_p = 0$). The geometry is a local Grad–Shafranov unshifted circular equilibrium generated using the Miller formalism [38,39]. All simulations retained 16 discrete complex toroidal modes

$$k_\theta \rho_s = 0.0,\ 0.05, 0.1,\ \ldots,\ 0.75 . \tag{37}$$

Both codes used a timestep of $(c_s/a)\Delta t = 0.04$. The binormal box size was fixed for all cases at $L_y \simeq 126\,\rho_s$. GYRO simulations used a nonperiodic radial domain size of $L \simeq 220\,\rho_s$ with 260 radial gridpoints. This included two radial buffer zones of width $9\rho_s$ each. The CGYRO simulations used a periodic radial domain size of $L \simeq 200\,\rho_s$ with 180 radial wavenumbers. We introduce an *effective magnetic field* $B_{\rm unit}$ [18,40], which is defined with reference to a global equilibrium through the relation

$$B_{\rm unit}(r) = \frac{q}{r}\psi' , \tag{38}$$

where ψ' is defined as $\partial\psi/\partial r$. In terms of $B_{\rm unit}$, we define an *effective ion-sound gyroradius*

$$\rho_s \doteq \frac{c_s}{eB_{\rm unit}/(m_D c)} . \tag{39}$$

For nonlinear simulations, because the energy and momentum fluxes have a natural gyroBohm scaling, we normalize them to a reference gyroBohm level

$$Q_{\rm GB} = n_e T_e c_s \frac{\rho_s^2}{a^2} \quad \text{and} \quad \Pi_{\rm GB} = n_e a T_e \frac{\rho_s^2}{a^2} \,. \tag{40}$$

References

[1] R. Waltz, G. Kerbel, J. Milovich, Toroidal gyro-Landau fluid model turbulence simulations in a nonlinear ballooning mode representation with radial modes, Phys. Plasmas 1 (1994) 2229.
[2] R. Miller, F. Waelbroeck, A. Hassam, R. Waltz, Stabilization of ballooning modes with sheared toroidal rotation, Phys. Plasmas 2 (1995) 3676.
[3] A. Dimits, T. Williams, J. Byers, B. Cohen, Scalings of ion-temperature-gradient-driven anomalous transport in tokamaks, Phys. Rev. Lett. 77 (1996) 71.
[4] R. Waltz, G. Staebler, W. Dorland, G. Hammett, M. Kotschenreuther, J. Konings, A gyro-Landau fluid transport model, Phys. Plasmas 4 (1997) 2482.
[5] R. Waltz, R. Dewar, X. Garbet, Theory and simulation of rotational shear stabilization of turbulence, Phys. Plasmas 5 (1998) 1784.
[6] J. Candy, R. Waltz, An Eulerian gyrokinetic-Maxwell solver, J. Comput. Phys. 186 (2003) 545.
[7] A. Dimits, Fluid simulations of tokamak turbulence in quasiballooning coordinates, Phys. Rev. E 48 (1993) 4070.
[8] N. Howard, A. White, M. Greenwald, M. Reinke, J. Walk, C. Holland, J. Candy, T. Görler, Investigation of the transport shortfall in alcator c-mod l-mode plasmas, Phys. Plasmas 20 (2013) 032510.
[9] N. Howard, C. Holland, A. White, M. Greenwald, J. Candy, Synergistic cross-scale coupling of turbulence in a tokamak plasma, Phys. Plasmas 21 (2014) 112510.
[10] F. Casson, A. Peeters, Y. Camenen, W. Hornsby, A. Snodin, D. Strinzi, G. Szepesi, Anomalous parallel momentum transport due to E×B flow shear in a tokamak plasma, Phys. Plasmas 16 (2009) 092303.
[11] G. Hammett, et al., Implementation of large scale E×B shear flow in the GS2 gyrokinetic turbulence code, Bull. Am. Phys. Soc. (2006) VP1.00136, http://meetings.aps.org/link/BAPS.2006.DPP.VP1.136.
[12] A. Peeters, Y. Camenen, F. Casson, W. Hornsby, A. Snodin, D. Strintzi, G. Szepesi, The non-linear gyrokinetic flux tube code GKW, Comput. Phys. Commun. 180 (2009) 2650.
[13] F. Casson, Turbulent Transport in Rotating Tokamak Plasmas, Ph.D. thesis, University of Warwick, 2011.
[14] H. Sugama, W. Horton, Transport processes and entropy production in toroidally rotating plasmas with electrostatic turbulence, Phys. Plasmas 4 (1997) 405.
[15] H. Sugama, W. Horton, Nonlinear electromagnetic gyrokinetic equation for plasmas with large mean flows, Phys. Plasmas 5 (1998) 2560.
[16] A. Brizard, Nonlinear gyrokinetic Vlasov equation for toroidally rotating axisymmetric tokamaks, Phys. Plasmas 2 (1995) 459.
[17] F. Hinton, S. Wong, Neoclassical ion transport in rotating axisymmetric plasmas, Phys. Fluids 28 (1985) 3082.
[18] J. Candy, A unified method for operator evaluation in local Grad–Shafranov plasma equilibria, Plasma Phys. Control. Fusion 51 (2009) 105009.
[19] M. Kruskal, R. Kulsrud, Equilibrium of a magnetically confined plasma in a toroid, Phys. Fluids 1 (1958) 265.
[20] J. Candy, E. Belli, R. Bravenec, A high-accuracy Eulerian gyrokinetic solver for collisional plasmas, J. Comput. Phys. 324 (2016) 73.
[21] R. Rogallo, Numerical Experiments in Homogeneous Turbulence, NASA Tech. Memo. 81315, 1981.
[22] A. Pumir, Turbulence in homogeneous shear flows, Phys. Fluids 8 (1996) 3112.
[23] J. Candy, E. Belli, GYRO Technical Guide, General Atomics Technical Report GA-A26818, 2010.
[24] K. Brucker, J. Isaza, T. Vaithianathan, L. Collins, Efficient algorithm for simulating homogeneous turbulent shear flow without remeshing, J. Comput. Phys. 225 (2007) 20.
[25] R. Buchholz, Y. Camenen, F. Casson, S. Grosshauser, W. Hornsby, P. Migliano, A. Peeters, Toroidal momentum transport in a tokamak due to profile shearing, Phys. Plasmas 21 (2014) 062304.
[26] J. Kinsey, R. Waltz, J. Candy, Nonlinear gyrokinetic turbulence simulations of E×B shear quenching of transport, Phys. Plasmas 12 (2005) 062302.
[27] J. Kinsey, R. Waltz, J. Candy, The effect of plasma shaping on turbulent transport and E×B shear quenching in nonlinear gyrokinetic simulations, Phys. Plasmas 14 (2007) 102306.
[28] G. Staebler, J. Kinsey, R. Waltz, A theory-based transport model with comprehensive physics, Phys. Plasmas 14 (2007) 055909.
[29] M. Kotschenreuther, G. Rewoldt, W. Tang, Comparison of initial value and eigenvalue codes for kinetic toroidal plasma instabilities, Comput. Phys. Commun. 88 (1995) 128.
[30] W. Dorland, F. Jenko, M. Kotschenreuther, B. Rogers, Electron temperature gradient turbulence, Phys. Rev. Lett. 85 (2000) 5579.
[31] F. Jenko, W. Dorland, M. Kotschenreuther, B. Rogers, Electron temperature gradient driven turbulence, Phys. Plasmas 7 (2000) 1904.
[32] C. Roach, I. Abel, R. Akers, W. Arter, M. Barnes, Y. Camenen, F. Casson, G. Colyer, J. Connor, S. Cowley, D. Dickinson, W. Dorland, A. Field, W. Guttenfelder, G. Hammett, R. Hastie, E. Highcock, N. Loureiro, A. Peeters, M. Reshko, S. Saarelma, A. Schekochihin, H. Wilson, Gyrokinetic simulations of spherical tokamaks, Plasma Phys. Control. Fusion 51 (2009) 124020.
[33] M. Barnes, F. Parra, A. Schekochihin, S. Cowley, C. Roach, Turbulent transport in tokamak plasmas with rotational shear, Phys. Rev. Lett. 106 (2011) 175004.
[34] G. Staebler, R. Waltz, J. Kinsey, Discoveries from the exploration of gyrokinetic momentum transport, Phys. Plasmas 18 (2011) 056106.
[35] R. Waltz, G. Staebler, W. Solomon, Gyrokinetic simulation of momentum transport with residual stress from diamagnetic level velocity shears, Phys. Plasmas 18 (2011) 042504.
[36] R. Miller, R. Waltz, On the nature of rotational shear stabilization in toroidal geometry and its numerical representation, Phys. Plasmas 1 (1994) 2835.
[37] J. Candy, Turbulent energy exchange: calculation and relevance for profile prediction, Phys. Plasmas 20 (2013) 082503.
[38] R. Miller, M. Chu, J. Greene, Y. Lin-Liu, R. Waltz, Noncircular, finite aspect ratio, local equilibrium model, Phys. Plasmas 5 (1998) 973.
[39] J. Candy, C. Holland, R. Waltz, M. Fahey, E. Belli, Tokamak profile prediction using direct gyrokinetic and neoclassical simulation, Phys. Plasmas 16 (2009) 060704.
[40] R. Waltz, R. Miller, Ion temperature gradient turbulence simulations and plasma flux surface shape, Phys. Plasmas 6 (1999) 4265.